A general approach to break the concentration barrier in single-molecule imaging

Anna B. Loveland, Satoshi Habuchi, Johannes C. Walter, and Antoine M. van Oijen

This document contains:

1. **Supplementary Figures 1-8 and Legends**
2. **Supplementary Tables 1-2**
3. **Supplementary Methods**

Supplementary Figure 1: *Spectral properties of mKikGR.*

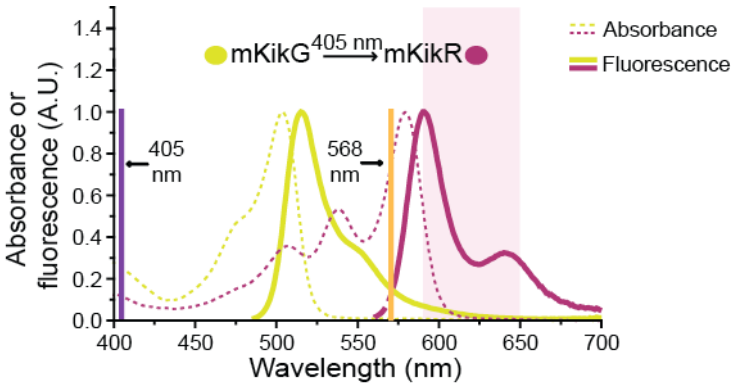

Wavelength dependence of absorbance (dashed lines) and fluorescence (solid lines) of mKikG (green) and mKikR (red) [1]. Photoactivation wavelength, λ_{act} = 405 nm (vertical purple line); mKikR excitation wavelength, λ_{ex} = 568 nm (vertical orange line); mKikR emission filter, 590-650-nm, (shaded region).

Supplementary Figure 2: *mKikGR is efficiently photoactivated.*

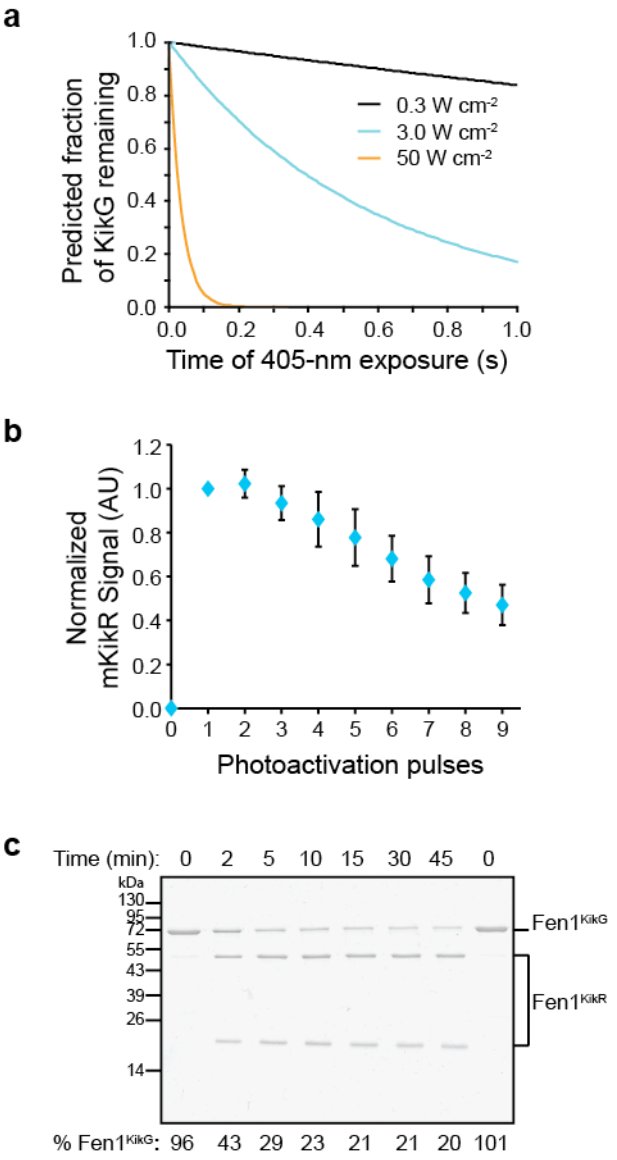

Supplementary Figure 2: (**a**) We first used the known photophysical properties of mKikGR [1] to calculate the predicted photoconversion efficiency of mKikG to mKikR. The efficiency of photoconversion, which we refer to as photoactivation, is dependent on the 405-nm irradiance (power, in units of W cm^{-2}) and its duration (in units of s). The decay constant for the loss of the green state (τ_p) can be derived for a particular irradiance using the following relation [2]:

$$\tau_p = \frac{1}{\Phi_p \cdot \sigma_\lambda \cdot I_\lambda\left(\frac{\lambda}{h \cdot c}\right)}, \qquad \text{(eq. 1)}$$

where Φ_p is the quantum yield of photoconversion of mKikGR, σ_λ is the absorption cross-section of the green state at wavelength λ, I_λ is the irradiance with λ, h is Planck's constant, and c is the speed of light. The values of the photoconversion quantum yield and the absorbance cross-

Supplementary Figure 2 continued

section of mKikG at λ = 405 nm have been previously measured: Φ_p = 7.5x10^{-3} and σ_{405} = 3.83x10^{-17} cm^2 at pH 7.5 [1]. Thus, the remaining fraction of mKikG (f_{KikG}) varies with the exposure time (t) and the calculated decay constant $\tau_p(I_{405})$ from eq. 1:

$$f_{KikG} = e^{\left(\frac{-t}{\tau_p}\right)}. \quad \text{(eq. 2)}$$

The plot shows the expected dependence of f_{KikG} on exposure time with varying values of irradiance (I_{405}): 0.3 W cm^{-2}, black line; 3.0 W cm^{-2}, blue line; 50 W cm^{-2}, orange line. For example, photoactivation for 400-ms pulse with 405-nm light at an irradiance of 3 W cm^{-2} is expected to yield ~50% photoactivation, while for 150 ms at 50 W cm^{-2} is expected to yield ~99% photoactivation. (**b**) The photoactivation efficiency of mKikGR was experimentally measured by repeated photoactivation and imaging of surface-immobilized Biotin-mKikR. The protein was imaged in ELB++ (see **Online Methods**) using multiple cycles of a 405-nm photoactivation pulse of 150 ms at 50 W cm^{-2}, followed by a 750-ms lag, and a 568-nm excitation pulse of 100 ms at 35 W cm^{-2}. The background-corrected, integrated intensity of Biotin-mKikR in a 100 μm^2 region was normalized to the intensity in the first post-activation frame and is shown plotted versus the number of photoactivation pulses. (Mean ± s.d, n = 5 independent experiments). The intensity of Biotin-mKikR does not significantly increase after the first photoactivation pulse, suggesting highly efficient photoactivation in the first pulse. The subsequent decay in signal is due to photodarkening of mKikR. (**c**) The photoactivation of KikG to KikR involves a beta elimination reaction that fragments the peptide backbone, allowing the extent of photoactivation to be monitored via SDS-PAGE [1]. A quartz cuvette containing a 0.1 mg ml^{-1} solution of WT Fen1^{KikGR} in 10 mM Hepes, 100 mM KCl, 2.5 mM $MgCl_2$ was irradiated with 405-nm light (0.01 W cm^{-2}). Before and at various times during exposure to 405-nm light, samples were withdrawn, separated on a 12% SDS-PAGE gel and stained with Coomassie Blue. The percentage of the fusion protein in the photoactivated state, Fen1^{KikR}, was measured via band densitometry of the two faster migrating protein bands and divided by the total signal in the three bands marked Fen1$^{KikG/R}$. 80% of the protein is eventually converted.

Supplementary Figure 3: *Characterization of Fen1^{KikGR}.*

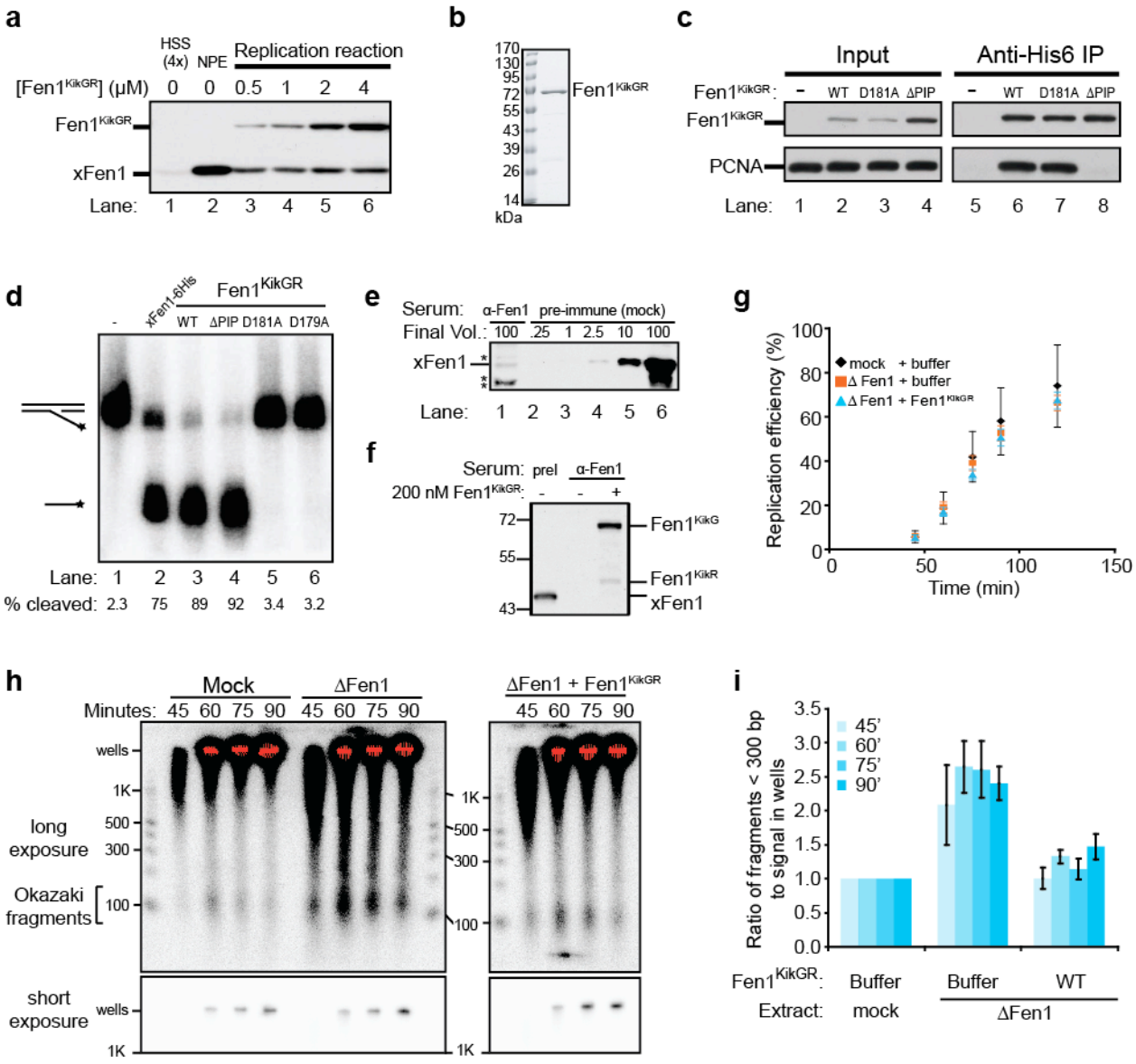

Supplementary Figure 3 (**a**) Comparison of a dilution series of purified Fen1^{KikGR} with egg extracts via Western blotting reveals that endogenous *Xenopus laevis* Fen1 is present at ~ 1 μM during replication. 0.8 μl of HSS, 0.2 μl of NPE or 0.2 μl of replication reactions (a 1:1:1 mixture of HSS, NPE, and supplements including DNA, proteins and buffer) containing the indicated final concentrations of WT Fen1^{KikGR} was analyzed by immunoblotting with anti-*Hs*Fen1 antibody. Note that Fen1 is highly enriched in NPE versus HSS. (**b**) 1 μg of purified WT Fen1^{KikGR} was separated by 10% SDS-PAGE and stained with Coomassie blue. (**c**) Specific binding of Fen1^{KikGR} to PCNA. HSS was supplemented with 1 μM WT or mutant Fen1-KikGR-6his proteins. Fen1^{KikGR} was immunoprecipitated from the HSS in each reaction with α-His6 antibody and the precipitate (lanes 5-8) was analyzed by immunoblotting with α-His6 and

Supplementary Figure 3 continued

xPCNA antibodies alongside 5% of the corresponding input (lanes 1-4). Note the absence of PCNA binding to Fen1 containing a mutated PCNA interaction protein (PIP) box motif (lane 8, ΔPIP Fen1^{KikGR}). (**d**) Flap cleavage activity of WT and mutant Fen1^{KikGR} proteins. 1 nM ^{32}P-labeled flap substrate was incubated with 100 nM WT Fen1-6his (lane 2, F6H) and WT or mutant Fen1^{KikGR} proteins (lanes 3-6) in the absence of $MgCl_2$ for 10 minutes at 22ºC. Next, the reactions were supplemented with 5 mM $MgCl_2$, incubated for 10 minutes at 22ºC, separated on 12% Urea-PAGE, and analyzed by phosphor imaging. The percentage of the ^{32}P-label found in the faster migrating species (% cleaved) is quantified below. (**e-i**) To investigate whether Fen1^{KikGR} is functional in DNA replication and Okazaki fragment maturation, we immunodepleted endogenous Fen1 from *Xenopus* egg extracts and replaced it with Fen1^{KikGR}. (**e**) *Xenopus* Fen1 antibody was used to immunodeplete Fen1 from egg extracts. The indicated amounts of Fen1-depleted or mock-depleted LSS (100 = 0.5 µl) were immunoblotted with anti-xFen1 antiserum. Fen1 depletion was ~97% efficient (compare lanes 1 and 4). *, non-specific bands. (**f**) Fen1-depleted LSS was supplemented with 200 nM Fen1^{KikGR}, which is roughly equivalent to the endogenous concentration of Fen1 in LSS. 0.2 µl of mock-depleted LSS, Fen1-depleted LSS (ΔFen1), or ΔFen1 LSS (from **Supplementary Fig. 3e**) supplemented with 200 nM WT Fen1^{KikGR} was immunoblotted with anti-xFen1 serum. (**g**) Fen1 depletion did not inhibit DNA replication in LSS. Replication of sperm chromatin (10,000 µl^{-1} final concentration) was measured in mock-depleted LSS, ΔFen1 LSS, and ΔFen1 LSS supplemented with 200 nM WT Fen1^{KikGR} (mean ± S.E.M, *n = 4*). (**h**) Denaturing agarose gels were used to examine the steady-state levels of Okazaki fragments in Fen1-depleted egg extracts. Sperm chromatin (10,000 µl^{-1}) was incubated with Mock-depleted LSS, ΔFen1 LSS, or ΔFen1 LSS supplemented with 200 nM WT Fen1^{KikGR}. At the indicated times, samples were withdrawn, and DNA was subjected to electrophoresis on two alkaline-agarose gels (2%) run side-by-side. A long phosphor imager exposure of the gels (top panels) was used to visualize short nascent strands, which includes Okazaki fragments (~120 bp) (bracket). The high MW nascent strands in the well saturated the phosphor screen (red), and a short exposure (bottom panels) was used to quantify these. Note that Fen1 depletion from LSS resulted in increase in Okazaki fragments during replication, and this increase was reversed by the addition of Fen1^{KikGR}. (**i**) Quantification of Okazaki fragments. The ratio of radioactivity in short (< 300 bp in size) and long (> 1,000 bp) DNA fragments (as in **Supplementary Fig. 3h**) was measured for each sample and normalized to the value of the mock-depleted control (mean ± s.e.m., *n = 4* except ΔFen1 time points 60 and 90 minutes, *n = 3)*.

Supplementary Figure 4: *PhADE detects the growth and initiation of replication bubbles with minimum perturbation to the replication program.*

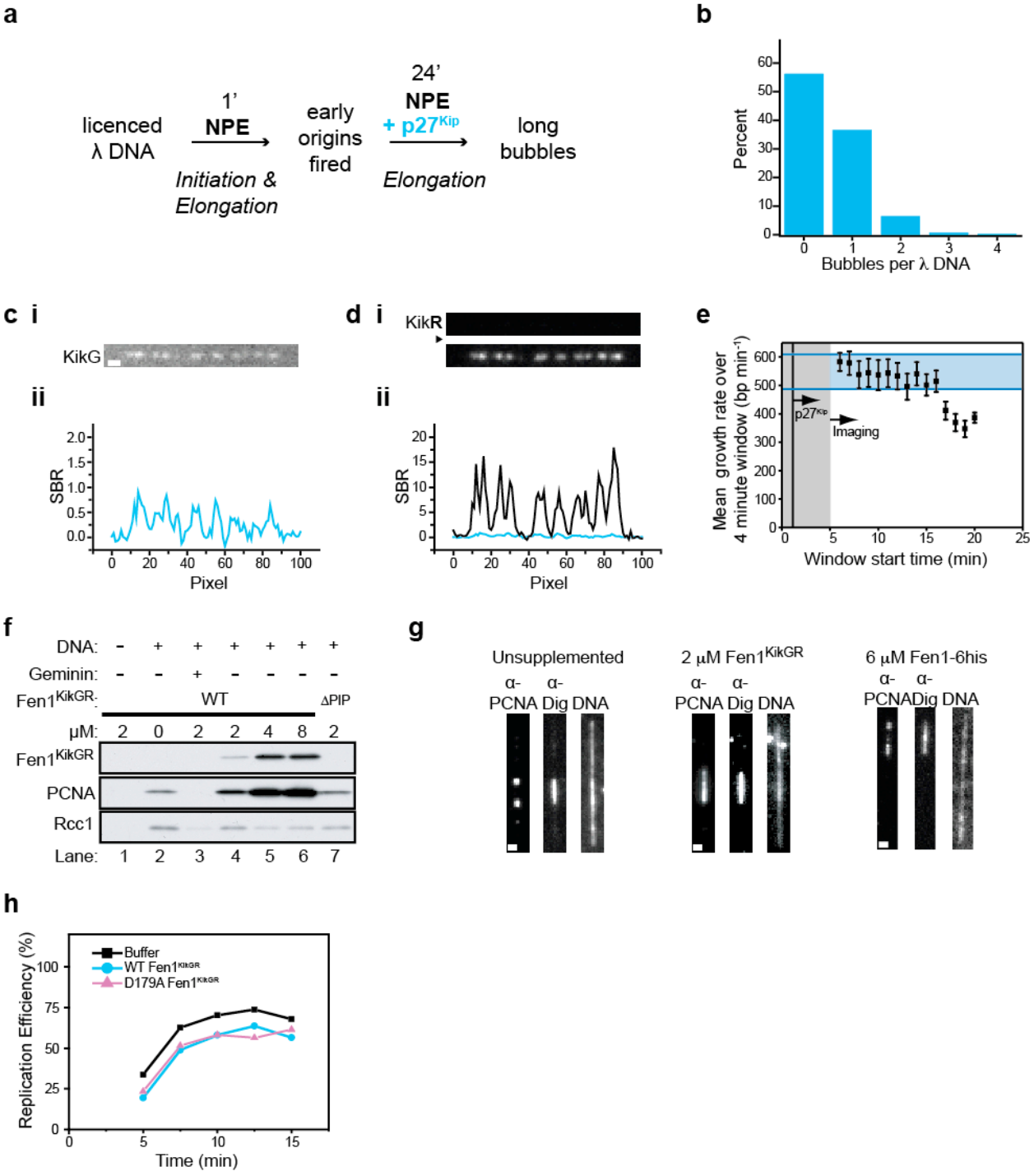

Supplementary Figure 4: (**a**) Experimental scheme using the Cdk2 inhibitor p27^{Kip} to restrict initiations to one event per λ DNA (see also Methods). (**b**) p27^{Kip} added one minute after NPE limits initiation. Following imaging of replication elongation in **Figure 2c**, replication bubbles

Supplementary Figure 4: continued

on λ DNA were detected by immunostaining of incorporated dig-dUTP. A histogram of the number of replication bubbles per λ DNA in fields that were not used for D179A Fen1^{KikR} imaging demonstrates that most λ DNAs underwent zero or one initiation event (n = 465 λ DNAs from three experiments). (**c-d**) PhADE enhances the contrast of features made up of multiple Fen1^{KikGR} molecules. (**c**) (i) Doubly-tethered λ DNA was assembled in a flow cell and licensed by introducing HSS for 20 minutes. Next, replication was initiated by introducing NPE supplemented with 2 μM D179A Fen1^{KikGR} and dig-dUTP. p27^{Kip} was not added in this experiment, allowing unrestricted origin firing. Fen1^{KikG} was imaged 16 minutes later with 488-nm excitation (100 ms, 3 W cm^{-2}). Scale bar: 1 μm. (ii) Profile of the signal-to-background ratio through the mKikG feature, where signal is defined as the total pixel intensity minus background pixel intensity. (**d**) (i) Fen1^{KikR} in the region from **Supplementary Figure 4ci** was imaged 12 s later with 568-nm excitation (100 ms, 3.5 W cm^{-2}; top panel), photoactivated with 405-nm light (400 ms, 3 W cm^{-2}; ~50% of molecules activated), and imaged again 1 s later (bottom panel). (ii) Profile of the signal-to-background ratio through Fen1^{KikR} from **Supplementary Figure 4di**, bottom panel (black) or Fen1^{KikG} (grey; same as in **Supplementary Fig. 4cii**). The comparison of **Supplementary Figures 4cii and 4dii** shows a much higher signal to noise ratio in the latter. (**e**) To learn whether repeated photoactivation and imaging of Fen1^{KikR} damages replication forks, we compared the rate of bubble growth in a field of view subjected to PhADE imaging (as in **Fig. 2c**) to an estimate of the growth rate in non-imaged fields. The replication bubble growth rate in non-imaged fields was estimated by dividing the mean size of bubbles in these fields (12,200 ± 900 bp (± error estimate)) by the time allowed for elongation (25 minutes). However, there is an uncertainty about the time of replication initiation in these non-imaged fields. Initiation may have occurred by the time of p27^{Kip} addition or been delayed by ~ 5 minutes, as observed for most bubbles imaged with PhADE (data not shown). Assuming that initiation occurred between 0 and 5 minutes after NPE addition and that elongation continued at a constant rate until 25 minutes, the non-imaged replication bubbles grew at a rate of 490-610 bp min^{-1} (blue horizontal zone). These values are consistent with the mean growth rate of 520 ± 220 bp min^{-1} rate measured from bubbles imaged in real time (**Fig. 2d**) suggesting that the imaging conditions used do not alter fork progression. Because damage from activation and imaging may accumulate over time, average rates derived from the entire imaging period may not reveal fork slowing towards the end of the experiment. Therefore, we analyzed the mean growth rate of PhADE-imaged replication bubbles as a function of time during 4-minute windows between 6 and 20 minutes (black squares). Only marginal slowing occurred after 12 minutes of imaging (after 72 frames or the 17 minute time point), indicating that photo-induced fork stalling was not significant when data collection was limited to fewer than 72 frames. (**f**) High concentrations of WT Fen1^{KikGR} enhance PCNA binding to DNA. Sperm chromatin (10,000 μl^{-1} final concentration) was licensed in HSS. Lane 1, no DNA control. The reaction in lane 3 included 400 nM geminin, an inhibitor of the licensing factor Cdt1, to prevent MCM2-7 loading and DNA replication [3,4]. After 30 minutes, 2 volumes of NPE were added to promote replication on the licensed chromatin along with WT (lanes 3 to 6) or PCNA-binding deficient (ΔPIP, lane 7) Fen1^{KikGR} at the indicated final concentrations. After a further 20 minutes, the sperm chromatin was isolated and chromatin-bound proteins were analyzed by immunoblotting with α-His6, xPCNA, and Rcc1 antibodies. The data show that addition of WT Fen1^{KikGR} stabilized PCNA on DNA (compare lane 2 with lanes 4-6). (**g**) While PCNA normally binds to the ends of replication

Supplementary Figure 4 continued

bubbles, addition of 2 μM D179A Fen1^{KikGR} leads to PCNA binding along their entire length. Replication was carried out under conditions of limited origin firing (as in **Supplementary Fig. 4a**) in extracts supplemented with buffer (left), 2 μM D179A Fen1^{KikGR} (middle) or 6 μM WT Fen1-6his (right). Subsequently, PCNA was detected via indirect immunostaining (see **Supplementary Methods**) and replication bubbles were detected with α-Dig and SYTOX. Only in the presence of D179A Fen1^{KikGR} was PCNA bound along the entire length of replication bubbles. (**h**) Fen1^{KikGR} does not inhibit plasmid DNA replication. 9 ng μl^{-1} pBS(–)KS II plasmid was licensed in HSS, then supplemented with two volumes of NPE containing ^{32}P-α-dATP and buffer, WT, or nuclease-deficient D179A Fen1^{KikGR} (final concentration 2 μM). ^{32}P-α-dATP incorporation was used to measure replication efficiency. A representative experiment is shown.

Supplementary Figure 5: *Fen1^{KikR} detects replication bubbles greater than 1 kbp to reveal the time and spacing of replication initiation.*

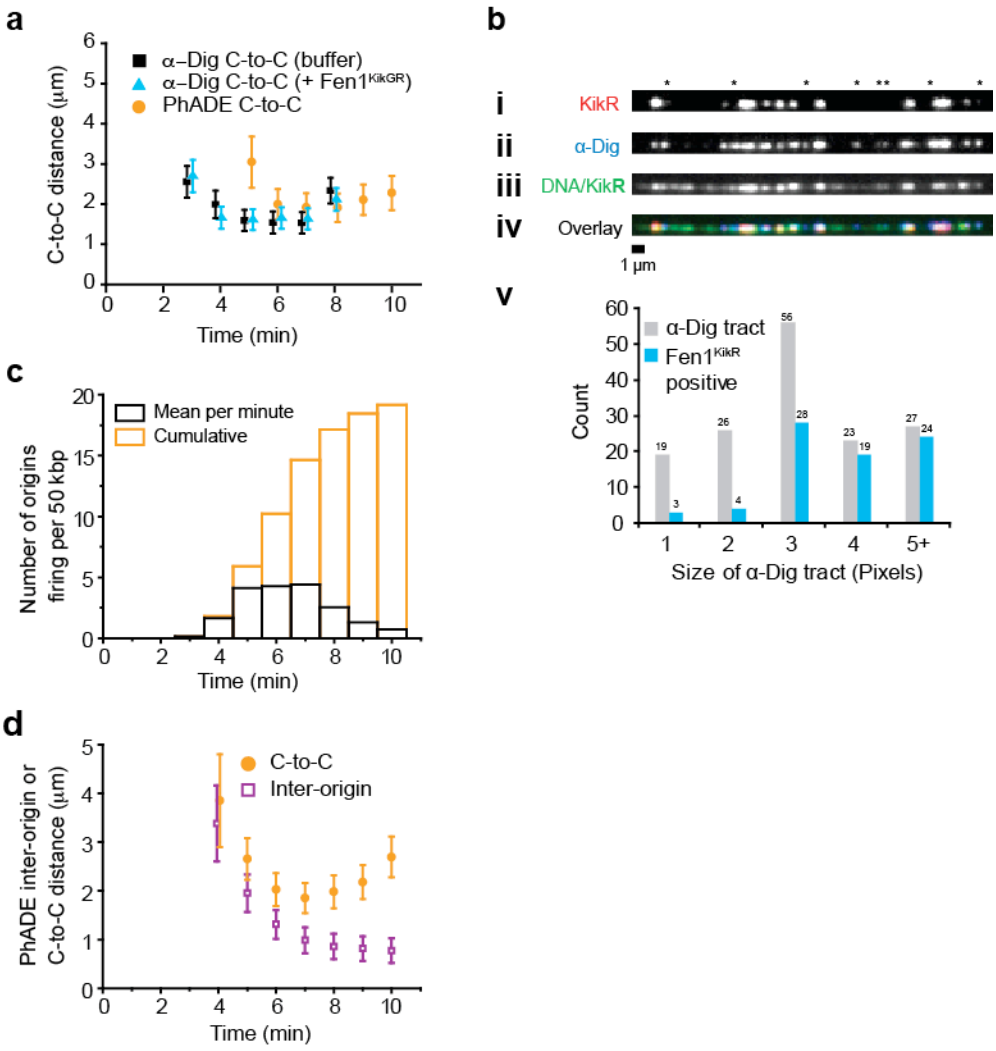

Supplementary Figure 5: (**a**) To confirm that all replication bubbles are detected via PhADE, we compared the replication profiles determined dynamically via PhADE, as in **Figure 3a**, to those determined from staining of Dig-dUTP incorporation. At equivalent times after NPE addition, we quantified the distances between the centers of neighboring replication bubbles (center-to-center, C-to-C distances) detected via D179A Fen1^{KikR} PhADE (orange circles) and α-Dig staining (black squares, buffer; blue triangles, 2 μM D179A Fen1^{KikGR}). The profiles from the PhADE movies essentially reproduce the α-Dig profiles, except for a ~2-minute delay. The delay is consistent with a bubble-growth rate of 520 ± 220 bp min^{-1} (**Fig. 2d**) and our observation that D179A Fen1^{KikR} only detects bubbles longer than 1 kbp (**Supplementary Fig. 5b** and data not shown). The similarity of the α-Dig and D179A Fen1^{KikR} profiles suggests that the latter eventually detects all bubbles and is a reliable readout for the dynamics of replication initiation and elongation. We also note that C-to-C distances as measured by α-Dig imaging are the same in the presence and absence of D179A Fen1^{KikGR} (compare black squares and blue triangles), further confirming that this protein has no adverse effects on replication dynamics.

Supplementary Figure 5 continued

(**b**) Replication bubbles greater than 1 kbp are detectable by D179A Fen1^{KikR}. λ DNA was replicated in the presence of 4 μM D179A Fen1^{KikGR}. Starting 2.5 minutes after NPE addition, D179A Fen1^{KikR} was imaged using cycles of PhADE every 5 seconds (Photoactivate: 405 nm, 3 W cm^{-2}, 400 ms; wait 4.5 s for diffusion; Image: 568 nm, 3.5 W cm^{-2}, 100 ms) for 3.5 minutes. (i) The last D179A Fen1^{KikR} frame in the presence of extracts is shown. (ii) After extract removal, the replicated DNA was stained with α-Dig. (iii) DNA was stained with SYTOX Orange. (iv) Overlay of the three channels. Asterisks (*) mark small α-Dig tracts not detected by D179A Fen1^{KikR}. (v) Images like those in i-iv were analyzed for α-Dig tracts, sorted by the size of the tracts, and graphed (grey columns). Next, each α-Dig tract was scored for the presence of D179A Fen1^{KikR} in the last frame prior to extract removal, and those tracts scoring positive were sorted by size and graphed (blue columns). Notably, α-Dig tracts that are 1 or 2 pixels (< 1kbp) long do not stain for D179A Fen1^{KikR}. D179A Fen1^{KikR} was detected on DNA in the absence of α-Dig < 2% of the time (not depicted in graph) and was absent from 4.5% of larger bubbles. Both events could reflect a shift of a compacted mass of DNA relative to the static tether points following D179A Fen1^{KikR} imaging but preceding α-Dig staining. (**c**) Same as in **Figure 3b** except using an independently prepared HSS and NPE and 4 μM D179A. (N = 35 λ DNA). (**d**) The center-to-center distance between bubbles increases at late time points during replication bubble merging, obscuring origin firing. The cumulative, inter-origin distance, which can be measured from PhADE movies but not static datasets, continues to decline during replication. Purple symbols same as in **Figure 3d** and orange symbols same as in **Supplementary Figure 5a** except using an independently prepared HSS and NPE and 4 μM D179A Fen1^{KikGR} that was also analyzed in **Supplementary Figure 5c**.

Supplementary Figure 6: *Fen1^{KikGR} localization to replication forks is concentration and PCNA dependent.*

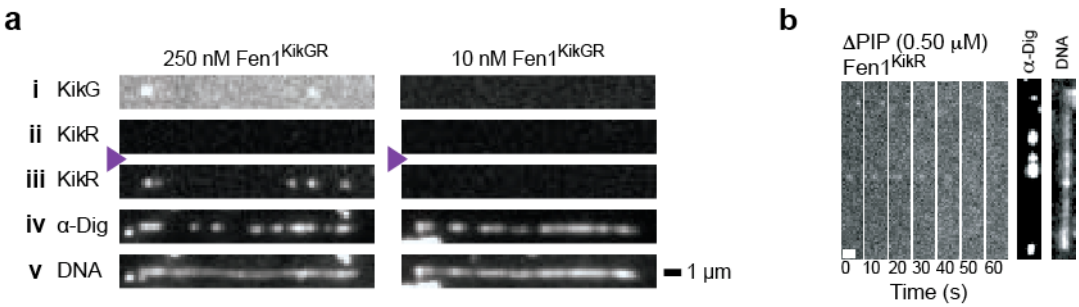

Supplementary Figure 6: (**a**) Fen1^{KikGR} is not detected at replication forks at concentrations compatible with conventional single-molecule imaging. Doubly-tethered λ DNA was replicated in the presence of 250 nM (left panels) and 10 nM (right panels) WT Fen1^{KikGR}. (i) Fen1^{KikG} was imaged during replication (488-nm excitation, 37 W cm^{-2}, 100 ms). (ii) Fen1^{KikR} in the region from (i) was imaged 10 s later (562-nm excitation, 47 W cm^{-2}, 100 ms). (iii) 700 ms after photoactivation (405 nm, 300 ms, 30 W cm^{-2}; ~90% of molecules activated), Fen1^{KikR} was imaged again. (iv) Immediately afterwards, extract was removed and replicated DNA was stained with α-Dig. (v) Total DNA was stained with an intercalating dye, SYTOX Orange. Note that at the lower concentration of Fen1^{KikGR}, no binding events were detected. This is likely due to the fact that at this concentration, WT Fen1^{KikGR} does not compete effectively with endogenous Fen1 for binding to DNA replication forks. (**b**) Fen1^{KikGR} localization to replication forks is dependent on interaction with PCNA. λ DNA was replicated in the presence of 0.5 μM PCNA-binding deficient (ΔPIP) Fen1^{KikGR} and imaged as in **Figure 4a-b**. Only 3 Fen1^{KikR} foci were detected on 46 replication bubbles.

Supplementary Figure 7: *Strategies to measure the Fen1^{KikR} off-rate from DNA.*

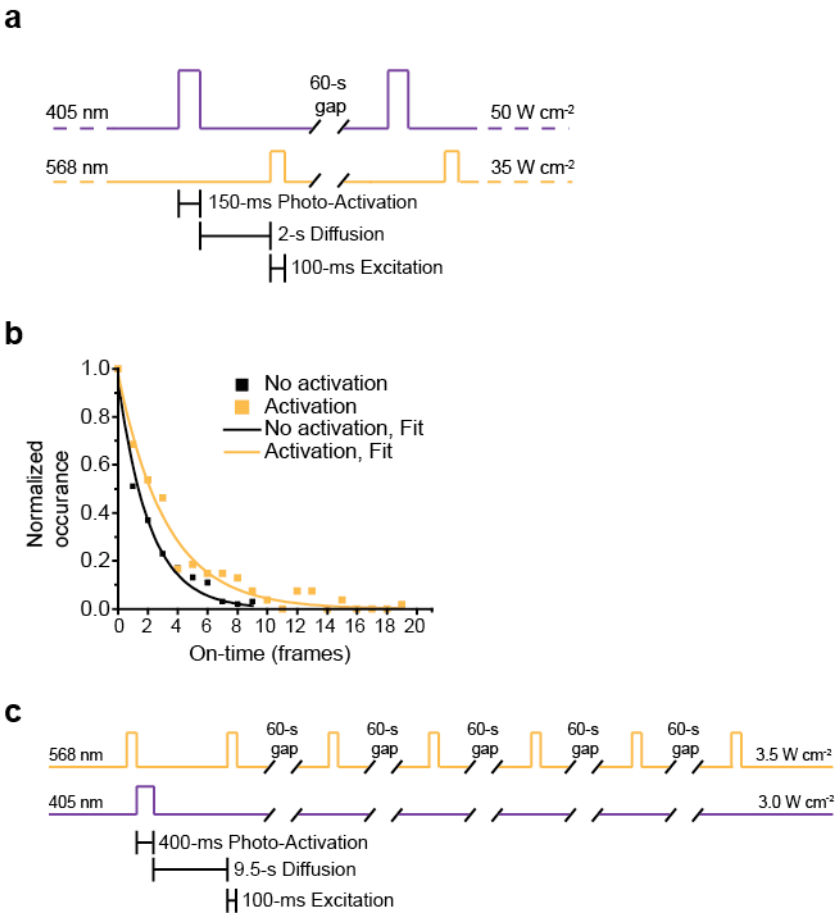

Supplementary Figure 7: (**a**) To determine the number of frames that a single Fen1^{KikR} molecule persisted on DNA ("on-time"), we used iterative cycles of PhADE imaging separated by one-minute waiting periods as shown in this scheme. Photoactivation efficiency was ~90% during each round (**Supplementary Fig. 2a**). Re-exposure to 405-nm light was found to keep previously activated molecules in the fluorescent state (**Supplementary Fig. 7b**) and allowed the same molecule to be imaged for more consecutive frames. Prolonging the fluorescent state in this manner is important because we define the "on-time" as the number of consecutive frames that a specific location on DNA remains fluorescent, and we compare this value to the photodarkening of a Biotin-KikR standard imaged in the same way. Of note, re-exposure of the sample to 405-nm light also activated new molecules that bound to DNA during the waiting time. If these new molecules were to bind in the same location as a molecule that had dissociated, the on-time measurement might reflect multiple Fen1^{KikR} binding events. However, given the low fractional occupancy of the replication bubbles by Fen1^{KikR} in each frame of these experiments (<25% in **Fig. 4d**), the likelihood of a new binding event at the same location is low (25% x 25% = 6.3%). Thus, the vast majority of observed binding events and the observed on times reflect single molecules of Fen1^{KikR} bound to DNA. (**b**) Reduction of mKikR photoblinking by re-exposure to 405-nm light. Single molecules of immobilized biotin-mKikGR were photoactivated (150 ms with 50 W cm^{-2} 405-nm light) once and mKikR was imaged (100 ms with 35 W cm^{-2} 568-nm excitation) every 500 ms thereafter, either in the absence of further photoactivation (black) or

Supplementary Figure 7 continued

with the same photoactivation pulse 250 ms before each image (orange). For those molecules that became fluorescent after the first photoactivation pulse, the number of consecutive frames in which the molecule stayed fluorescent was measured and is plotted here as the on time. The distribution of on times was well-fitted by a single-exponential decay in the presence of further photoactivation (mean life time of 3.2 ± 0.2 frames) and in its absence (mean life-time of 2.1 ± 0.2 frames). (C) PhADE imaging sequence used for **Figure 4f-g**.

Supplementary Figure 8: *High origin density does not result from limited chromatinization of λ DNA.*

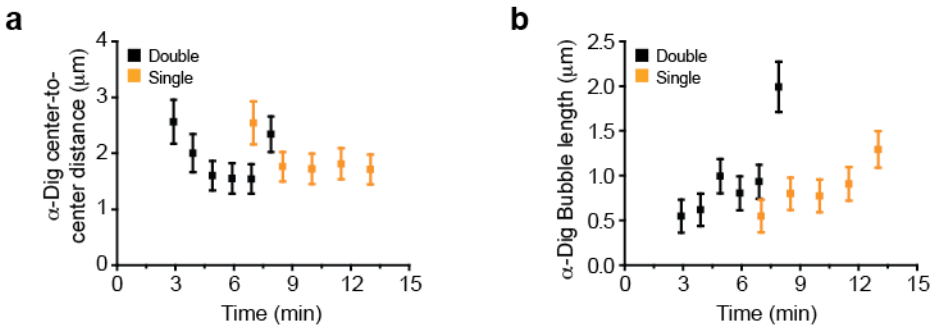

Supplementary Figure 8: (**a-b**) Given the limited slack present in the doubly-tethered λ DNA (~20%), maximally 20% of the DNA can be chromatinized. Therefore, a possible interpretation of the small inter-origin distance detected during PhADE imaging is that it results from incomplete chromatinization of the DNA template. To test this idea, we compared the static replication profiles of singly-tethered (unconstrained, presumably fully chromatinized) and doubly-tethered (constrained, partially chromatinized) λ DNA molecules. (**a**) Licensed, doubly-tethered (black, same as in **Supplementary Fig. 5a**) or singly-tethered (orange) λ DNA was exposed to NPE containing dig-dUTP for 2 to 13 minutes. At the indicated times, reactions were stopped and replication intermediates were detected with α-Dig and the center-to-center distance between neighboring bubbles was measured (mean ± error estimate) and graphed. There was little difference in minimum C-to-C distances between singly-tethered and doubly-tethered molecules. Interestingly, the minimum C-to-C distance was delayed by 5 minutes on the unconstrained molecules, implying that chromatin structure affects replication timing, possibly by delaying access of one or more initiation factors to the DNA. (**b**) The replication bubble lengths were measured as in **Supplementary Fig. 8a** and graphed (black, same data as in **Fig. 2e**). The data show that there was little difference in the length of α-Dig tracts. These observations suggest that chromatin structure does not affect fork rate or spacing of initiations in this system. As seen for the C-to-C distances, there was a 5-minute delay in bubble growth on singly-tethered versus doubly-tethered DNA. Our results therefore suggest that chromatin structure affects temporal but not spatial parameters of origin firing.

SUPPLEMENTARY TABLES

Supplementary Table 1: *Replication profiles of doubly-tethered λ DNA in the presence or absence of 2 μM D179A Fen1^{KikGR}.*

	Buffer			with 2μM Fen1-KikGR (D179A)		
Time	Mean	St. Dev.	Number	Mean	St. Dev.	Number
% Fiber Replicated						
3	14	9	53	14	6	57
4	32	9	59	45	1	62
5	61	8	78	55	9	111
6	51	12	62	59	10	86
7	59	9	66	65	9	97
8	82	10	42	76	8	81
Bubbles per Lambda DNA (48.5kb)						
3	3.3	1.9	53	3.4	1.6	57
4	6.4	2.0	59	7.1	1.5	62
5	7.7	1.5	78	7.5	1.5	111
6	7.8	2.1	62	7.4	1.7	86
7	8.0	1.5	66	7.7	1.5	97
8	5.1	1.5	42	5.9	1.5	81
Bubble size (μm)						
3	0.55	0.25	174	0.53	0.17	193
4	0.62	0.30	371	0.80	0.46	439
5	0.99	0.63	603	0.94	0.58	833
6	0.80	0.53	482	1.00	0.73	640
7	0.93	0.60	527	1.07	0.71	744
8	1.99	1.64	213	1.61	1.25	479
Center-to-center (μm)						
3	2.56	1.79	127	2.70	1.95	137
4	2.00	1.90	320	1.67	0.80	377
5	1.60	0.65	525	1.62	0.67	722
6	1.55	0.81	420	1.66	0.74	554
7	1.54	0.66	461	1.64	0.69	647
8	2.34	1.09	171	2.12	0.94	398

Supplementary Table 1: For each time point of the experiments presented in **Figure 2e** and **Supplementary Figure 5a**, > 50 λ DNA molecules (> 2.43 Mbp of DNA) were analyzed for the average % replication, number of bubbles per DNA, size of the bubbles (μm), and the center-to-center distances between adjacent bubbles (μm).

Supplementary Table 2: *Replication profiles of singly-tethered λ DNA*.

	Buffer		
Time	Mean	St. Dev.	Num
% Fiber Replicated			
7	14	10	72
8.5	42	13	146
10	43	10	82
11.5	47	15	85
13	71	9	89
Bubbles per Lambda DNA (48.5kb)			
7	3.4	2.1	72
8.5	6.9	1.6	146
10	7.2	1.3	82
11.5	6.5	1.7	85
13	7.1	1.7	89
Bubble size (μm)			
7	0.55	0.27	253
8.5	0.80	0.48	1010
10	0.77	0.39	587
11.5	0.91	0.52	556
13	1.29	0.94	631
Center-to-center (μm)			
7	2.54	1.99	181
8.5	1.76	0.83	861
10	1.72	0.85	505
11.5	1.81	0.93	472
13	1.71	0.73	542

Supplementary Table 2: For each time point of the experiment presented in **Supplementary Figure 8**, > 50 λ DNA molecules (> 2.43 Mbp of DNA) were analyzed for the average % replication, number of bubbles per DNA, size of the bubbles (μm), and the center-to-center distances between adjacent bubbles (μm).

SUPPLEMENTARY METHODS

Cloning and site-direct mutagenesis

Fen1-6his for antibody production was cloned as follows. *Xenopus laevis* Fen1a (xFen1) was amplified from pET28 2xFLAG-Fen1-GST-His [5] using primers C (5′-CTA TCC ATG GGA ATT CAC GGT TTG GCC AAA C-3′) and E (5′-TTT TCT CGA GTT AAT GAT GGT GAT GTT GAT GTT TAC CCC TCT TGA ACT TTC CTG C-3′) (IDT DNA) with flanking restriction sites and a C-terminal 6xhis tag, and the double digest was cloned into pET28b between the NcoI and XhoI sites. The ORF of the resulting plasmid pET28b-xFen1-6xhis was verified by sequencing (GeneWiz).

Egg Extract and Immunological Methods

High-speed supernatant (HSS) extract, nucleoplasmic extract (NPE), low-speed supernatant (LSS) and sperm chromatin were prepared from unfertilized *Xenopus laevis* eggs as described previously [6,7]. Chromatin spin-downs and bulk replication assays were performed as previously described [7,8]. For Western blotting, we used previously described antibodies against *Xl*RCC1 [9], *Xl* PCNA [10], *Hs* PCNA (Santa Cruz sc-056), *Hs*Fen1 (Cell Signaling Technology) [5] and 6His Tag (AbDSerotec MCA1396). For xFen1 antibody production, the xFen1-6his fusion protein, was expressed from plasmid pET28b-xFen1-6xhis and purified under the native conditions described in the **Online Methods** for Fen1-KikGR. xFen1-6his was used to generate polyclonal antibodies in rabbits (Pocono Rabbit Farm and Laboratory; Canadensis, PA). α-xFen1 serum but not the pre-immune serum recognized a band 45 kDa in size in LSS (data not shown).

PCNA binding assay

10 μL HSS, supplemented with 1 μM Fen1^{KikGR} WT or various Fen1^{KikGR} mutants, was incubated for 10 minutes at 22 ºC. The reaction was then diluted 50% with Binding Buffer (10 mM Hepes-KOH pH 7.7, 100 mM KCl, 2.5 mM $MgCl_2$ and 0.6% Triton X) and incubated with 5 μl of rProtein-A-Sepharose resin (GE Healthcare) cross-linked with DMP to 1 μg of α-6His monoclonal antibody (MCA1396, AbDSerotec) for 30 minutes at 22 ºC. The beads were washed three times for one minute with 10 volumes of Binding Buffer, and bound proteins were analyzed by immunoblotting with α-His and α-xPCNA antibodies.

Flap endonuclease assay

The flap substrate was prepared using oligonucleotides (IDT DNA) as described in [11]. 2.5 pmol of the "Flap strand" was end-labeled by T4 PNK (NEB) with ^{32}P-γ-dATP (Perkin-Elmer). Free, labeled nucleotides were removed by gel filtration (illustra ProbeQuant^{TM} G-50 Micro Columns, GE Healthcare). 5 pmol of "F_{br} strand" and "F_{adj} strand" were added and annealed in 50 μL of STE (10mM Tris 7.5, 50mM NaCl and 0.1mM EDTA) by heating to 95ºC and slow cooling to room temperature. For the cleavage assay [12], 2 fmol of flap substrate was incubated with 0.2 pmol of Fen1 WT or mutant protein in a total volume of 20 μl of Flap Binding Buffer (50 mM Tris 8, 30 mM NaCl, 5% Glycerol, 2mM DTT, 0.2 mg ml^{-1} BSA and 1mM EDTA) for 10 minutes at room temperature. Next, the reaction was supplemented with 1/10 volume of 50 mM $MgCl_2$ and incubated a further 10 minutes at room temperature. The reactions were stopped with Gel Loading Buffer II (Ambion), heated to 80ºC for 5 minutes, and separated on 12% Urea-PAGE mini-gels at 20W for ~20 minutes. The fate of the ^{32}P-labeled flap strand was determined by phosphor imager analysis.

xFen1 depletion and nascent strand assay

To deplete Fen1 from LSS, 1 volume of rProtein-A Sepharose Fast Flow resin (GE Healthcare) was incubated with 3 volumes α-xFen1 or matched pre-immune serum (mock control) for 30 minutes at 4ºC. The beads were washed 4 times with 500 µl PBS and 2 times with ELB (10 mM Hepes-KOH 7.7, 50 mM KCl, 2.5 mM $MgCl_2$, 250 mM Sucrose). Next, one volume of LSS supplemented with 3.3 ng μl^{-1} nocodazole was incubated with 0.2 volumes of antibody-bound beads for 30 minutes at 4ºC. Beads were spun down, LSS in the supernatant was collected, and the depletion procedure was repeated once. After the final round, LSS was isolated from beads by spinning through Nitex membrane and was immediately used for DNA replication.

Mock- or Fen1-depleted LSS was supplemented with an ATP regeneration system (2 mM ATP, 20 mM phosphocreatine, 5 µg ml^{-1} creatine kinase), $Fen1^{KikGR}$ or Fen1 storage buffer, ^{32}P-α-dATP, and 10,000 sperm μl^{-1}, and reactions were moved to 22ºC to start replication. At the appropriate time, samples were withdrawn and processed differentially either for native agarose gels to determine replication efficiency [7] or denaturing agarose gels to visualized the size distribution of nascent strands [13]. For the latter, 2 µl aliquots of the reaction were transferred into 200 µl of ice-cold Buffer A (20 mM Hepes-KOH, pH 7.6, 50 mM NaCl, 5mM EDTA) supplemented with 1 mM spermidine and 1 mM spermine. After all time points were collected, the reactions were centrifuged 5 minutes at 4ºC. Pellets were resuspended in Buffer A supplemented with 0.5% SDS and 0.1 mg ml^{-1} RNase A to digest single-stranded RNA and incubated for 30 minutes at 37ºC. 0.5 mg ml^{-1} proteinase K was added to digest proteins for one hour at 37ºC. Finally, DNA was extracted with phenol:chloroform and ethanol precipitated in the presence of 10 µg of glycogen. DNA Pellets were resuspended in Alkaline Agarose Loading Buffer (100 mM NaOH, 1mM EDTA, 5% Ficoll 400, and 0.025% Bromocresol Green) and run immediately on a 2% alkaline agarose gel alongside a ^{32}P-labeled 100 bp ladder (NEB), 2 V cm^{-1} for 18 hours. Gels were dried between DE81 paper (Whatman) and exposed to a phosphor screen. A one hour exposure was used to quantify the abundant large nascent strands running greater than 1,000 bp. A 36 hour or longer exposure was needed to quantify the short nascent strands running < 300 bp in size.

α-Dig staining and measuring of replication bubbles on doubly and singly-tethered DNA

To image replication intermediates on singly- verus doubly-tethered λ DNA, slightly different procedures were used. For singly-tethered DNA, extracts and proteins compacting the DNA were removed by flow of 1 x PBS with 0.1% SDS, initially at 10 µl min^{-1} for 5 minutes then 50 µl min^{-1} for 5 minutes to stretch the DNA. SDS was then removed with a 1 minute wash with 1 x PBS. For studying replication on doubly-tethered λ DNA, extracts but not all proteins bound to DNA were removed by flushing the flow cell with ELB++ for at total of 10 minutes at 10 µl min^{-1}. Under these conditions, singly-tethered DNA remained compacted while doubly-tethered DNA remained extended. Next, dig-dUTP incorporation on singly-tethered or doubly-tethered λ DNA was stained with anti-digoxigenin-fluorescein Fab fragments (α-Dig) (Roche) and co-stained with SYTOX Orange (Invitrogen). Doubly-tethered DNA was imaged in the absence of flow while singly-tethered DNA was imaged at a flow rate of 100 µl min^{-1} of the SYTOX Orange solution to stretch the DNA. α-Dig was excited with 488-nm light (2.3 W cm^{-2}, 100 ms) and SYTOX Orange was excited with 568-nm light (3.5 W cm^{-2}, 100 ms).

Immunostaining of PCNA at individual replication forks

Following λ DNA replication in the flow cell, extracts were removed by washing with Wash Buffer 2 (10 mM Hepes 7.7, 300 mM KCl, 2.5 mM $MgCl_2$ with 0.1mg ml^{-1} BSA) for 5 minutes at 20 µl min^{-1}. The flow-cell surface was further washed and blocked by flow of ELB++ for 25 minutes, 20 µl min^{-1}. Next, Dig-dUTP incorporation was stained as described above. After washing with ELB++ for 5 minutes, PCNA was stained as follows. First 1.2 ng $µl^{-1}$ α-*Xl*PCNA IgG in ELB++ (purified from serum on rProtein-A Sepharose Fast Flow resin (GE Healthcare)) was introduced into the flow cell at 10 µl min^{-1} for 15 minutes. After washing with ELB++ for 5 minutes, the α-xPCNA rabbit IgG was detected with 2ng $µl^{-1}$ Goat-anti-Rabbit IgG-AlexaFluor647 (Invitrogen) in ELB++, introduced into the flow cell at 10 µl min^{-1} for 5 minutes. Free secondary antibody was removed by flushing the flow cell with ELB++ at 10 µl min^{-1} for 5 minutes. Lastly, DNA was stained with SYTOX Orange as described above. α-Dig and SYTOX were detected as before. The α-PCNA signal was excited with 647-nm light (0.16 W cm^{-2}, 100 ms exposure).

SUPPLEMENTARY REFERENCES

1. Habuchi, S., Tsutsui, H., Kochaniak, A.B., Miyawaki, A. & van Oijen, A.M. mKikGR, a monomeric photoswitchable fluorescent protein. *PLoS ONE* **3**, e3944 (2008).
2. Thompson, M.A., Biteen, J.S., Lord, S.J., Conley, N.R. & Moerner, W.E. Molecules and Methods for Super-Resolution Imaging. in *Single Molecule Tools, Part B:Super-Resolution, Particle Tracking, Multiparameter, and Force Based Methods* (ed. Walter, N.G.) 2: 27-59 (Academic Press, 2010).
3. Wohlschlegel, J.A. et al. Inhibition of eukaryotic DNA replication by geminin binding to Cdt1. *Science* **290**, 2309-2312 (2000).
4. Tada, S., Li, A., Maiorano, D., Mechali, M. & Blow, J.J. Repression of origin assembly in metaphase depends on inhibition of RLF-B/Cdt1 by geminin. *Nature Cell Biol* **2**, 107-113 (2001).
5. Havens, C.G. & Walter, J.C. Docking of a Specialized PIP Box onto Chromatin-Bound PCNA Creates a Degron for the Ubiquitin Ligase CRL4Cdt2. *Mol. Cell* **35**, 93-104 (2009).
6. Walter, J., Sun, L. & Newport, J. Regulated chromosomal DNA replication in the absence of a nucleus. *Mol. Cell* **1**, 519-529 (1998).
7. Lebofsky, R., Takahashi, T. & Walter, J.C. DNA replication in nucleus-free Xenopus egg extracts. *Methods Mol. Biol* **521**, 229-252 (2009).
8. Arias, E.E. & Walter, J.C. Replication-dependent destruction of Cdt1 limits DNA replication to a single round per cell cycle in Xenopus egg extracts. *Gene Dev.* **19**, 114-126 (2005).
9. Dasso, M., Nishitani, H., Kornbluth, S., Nishimoto, T. & Newport, J.W. RCC1, a regulator of mitosis, is essential for DNA replication. *Mol. Cell. Biol.* **12**, 3337-3345 (1992).
10. Kochaniak, A.B. et al. Proliferating cell nuclear antigen uses two distinct modes to move along DNA. *J. Biol. Chem.* **284**, 17700-17710 (2009).
11. Harrington, J.J. & Lieber, M.R. The characterization of a mammalian DNA structure-specific endonuclease. *EMBO J.* **13**, 1235-1246 (1994).
12. Gloor, J.W., Balakrishnan, L. & Bambara, R.A. Flap Endonuclease 1 Mechanism Analysis Indicates Flap Base Binding Prior to Threading. *J. Biol. Chem.* **285**, 34922-34931 (2010).
13. Walter, J. & Newport, J.W. Regulation of replicon size in Xenopus egg extracts. *Science* **275**, 993-995 (1997).
14. Bibikova, M. et al. Characterization of FEN-1 from Xenopus laevis. *J. Biol. Chem.* **273**, 34222-34229 (1998).
15. Walter, J.C. Evidence for sequential action of cdc7 and cdk2 protein kinases during initiation of DNA replication in Xenopus egg extracts. *J. Biol. Chem.* **275**, 39773-39778 (2000).